Engineered Science
DOI: https://dx.doi.org/10.30919/es996

Monodispersed Hollow Silica Nanospheres with Ultra-small Size for Fabrication of Highly Transparent Polymer Nanocomposites

Cai Li,[1] Xiao-Feng Pei,[2] Na Xiao[1] and Xiao-Fei Zeng[1, 2,*]

Abstract

Hollow silica nanospheres (HSNs) have been widely used as the antireflection coatings due to their low refractive index. However, it is difficult to incorporate them into optical polymer matrices to enhance the visible transmittance obviously using a simple blending method. Rayleigh scattering caused by their larger particle size and agglomerations problem would make the haze and transparency of optical polymer worse. Herein, ultra-small HSNs with the diameter of about 20 nm were synthesized by a reverse microemulsion method. The scale-up preparation was achieved by the high-gravity technology in a rotating-packed-bed reactor (RPB), and then a transparent polyvinyl alcohol (PVA)/HSNs nanocomposite was fabricated via a simple solution blending method. HSNs have an inner cavity size of about 8 nm and the refractive index is 1.342. They can be monodispersed in water and organic solvents respectively by using the different surface modifiers. The prepared PVA/HSNs nanocomposite has a super-high transparency and a low haze, resulting from that HSNs are homogeneously dispersed in PVA matrix without any aggregations, which has great application prospects in optical materials and devices.

Keywords: Hollow silica nanospheres; Reverse microemulsion; Rotating-packed-bed; Refractive index; Anti-reflection function.
Received: 01 September 2023; Revised: 18 October 2023; Accepted: 19 October 2023.
Article type: Research article.

1. Introduction

With the rapid development of nanotechnology, the emergence of nanomaterials with a hollow structure has impelled the application of nanomaterials in the different fields.[1-5] Among them, hollow silica nanospheres (HSNs) have been widely applied in diverse engineering and technological domain including optical, catalysis and biomedical materials.[6-8] Especially for the optical materials, HSNs with a low refractive index act as the anti-reflection additive or coating to enhance the visible transmittance of materials effectively. Introducing HSNs into polymer matrices can prepare the super transparent inorganic/organic nanocomposites, which have a significant application prospect in optical transmission, optical storage, and photoelectric display.[9-11]

HSNs have been generally synthesized by templating methods, which are further divided into three categories including self-template, soft template and hard template.[12-14] Among them, the third method is the most well-defined and has been widely applied in the preparation of HSNs.[12] Jia *et al*.[15] synthesized HSNs with diameter of 50 nm by using poly (acrylic acid) as a template, ethyl orthosilicate as a precursor respectively. The average transmittance of antireflective layer reached 99% in the wavelength from 380 to 1600 nm. Zhang *et al*.[8] prepared poly (acrylic acid)-silica nanospheres with a core-shell structure and then obtained HSNs by removing core. The particle size of the product was about 30 nm with obvious hollow structure, which is suitable for anti-reflection coating on solar glass of photovoltaic modules. However, in order to arrange HSNs evenly and improve the transparency remarkably, these antireflective layers with thin thickness were usually formed by the layer-by-layer self-assembly

[1] *State Key Laboratory of Organic-Inorganic Composites, Beijing University of Chemical Technology, Beijing 100029, PR China.*
[2] *Research Center of the* Ministry *of Education for High Gravity Engineering and Technology, Beijing University of Chemical Technology, Beijing 100029, PR China.*
**Email:* zengxf@mail.buct.edu.cn (X. F. Zeng)

method, which is time-consuming and complicated. Fabrication of anti-reflection inorganic/organic nanocomposites with high transparency by the simple blending method is rarely reported, because HSNs are easy to agglomerate and hard to be well dispersed in organic matrices by this method. According to the Rayleigh scattering principle, when the reflective index of HSNs is different from the polymer matrices, particles or particles aggregations with the size over 40 nm in optical materials can cause the light scattering.[16] HSNs can theoretically decrease the refractive index of transparent polymer to reduce the surface reflection, whereas they can also increase the light scattering inside the polymer caused by their larger grain size or agglomerations, resulting in that the haze is increased obviously and the total visible-light transmittance may be decreased. Therefore, the synthesis of ultrafine and well-dispersed HSNs is particularly important for the inorganic/organic optical nanomaterials.

In this paper, we have synthesized HSNs by a water-in-oil microemulsion method in the rotating-packed-bed (RPB) reactor, and then fabricated HSNs/PVA nanocomposite film via the solution blending method. RPB can generate a high-gravity environment to provide an excellent micromixing and mass transfer efficiency, contributing to generating faster nucleation rate and more uniform spatial concentration.[17] Hence, the prepared HSNs have a uniform hollow structure and a small size of about 20 nm. They can be monodispersed in water and some organic solvents respectively by modifying with the different surfactants. The refractive index of HSNs is 1.342. Nanoparticles can be well-dispersed in PVA matrix to reduce the reflection and therefore boost the visible transmittance from 91.5% to 98%. Meanwhile the haze is barely increased.

2. Experiment Section

2.1 Materials

Zinc acetate dihydrate ($Zn(Ac)_2 \cdot 2H_2O$), potassium hydroxide (KOH), methanol (MeOH), ethanol (EtOH), Cyclohexane, 3-aminopropyltriethoxysilane (KH550), 3-methacryloxypropyltrimethoxy- silane (KH570), 3-mercaptopropyltrimethoxysilane (KH590), polyethylene pyrrolidone (PVP), and methyl orthosilicate (TMOS) were purchased from Beijing Tongguang Fine Chemical Co. LTD. Ammonia ($NH_3 \cdot H_2O$, 28.0%), methyl isobutyl ketone (MIBK), polyvinyl alcohol (PVA) and polyoxyethylene(9)nonylphenyl ether (Igepal CO-630) were supplied by Tianjin Damao Chemical Reagent Factory. Deionized water was made by Beijing University of Chemical Technology. All of the reagents were of analytical purity and could be used directly.

2.1 Preparation of ZnO nanoparticles for template

425 mL $Zn(Ac)_2 \cdot 2H_2O$ methanol solution (0.4 M) were stirred at 400 rpm and heated at 70 °C for 10 min, followed by equivalent KOH ethanol solution (0.8 M) poured into a three-neck flask within 30 s. After reaction for 10 min, 2.1 g TMOS and 7 g KH550 were dropwise added successively with interval of 30 min. After 2 h surface modification, the obtained product was washed by ethanol, and dried by rotary evaporation. Finally, they were dispersed in deionized water and the transparent ZnO aqueous phase nanodispersion was achieved.

2.2 Preparation of Hollow Silica nanospheres (HSNs)

First, oil phase (100 g Igepal CO-630, 0.9 L cyclohexane and 4 mL TMOS) and aqueous phase (5 mL 10 wt% ZnO dispersion, 3 mL ammonia and 4 mL deionized water) were pumped into the RPB with flow rates of 250 and 2 mL/min respectively. Then reaction process proceeded for some time, followed by the modifier added to modify. After the reaction was over, the HSNs were precipitated and washed with ethanol, and then dispersed in the solvent to obtain the corresponding dispersions. In this study, the product modified by PVP, KH570, and KH590 would be dispersed in deionized water, MIBK, and MeOH respectively. In addition, the same process above was performed in stirring tank reactor (STR) for comparation. The oil phase and aqueous phase were slowly mixed in a beaker on the premise of magnetic stirring at 500 rpm and other conditions remained unchanged.

2.3 Preparation of HSNs/ PVA Composite Materials

Transparent PVA/HSNs nanocomposite films with low refractive index were fabricated by a facile solution mixing method. Typically, PVA was first dissolved in the deionized water at 90 °C under vigorous stirring for 2 h to obtain homogeneous solution. Subsequently, transparent PVP-modified HSNs nanodispersions with different HSNs content were added into the above PVA solution. The formed mixture was mixed and stirred in a flask for 30 min until a homogeneous and transparent solution was obtained. Finally, the above PVA/HSNs solution were placed in mold with vacuum drying at 40 °C for 72 h. Finally, the HSNs/PVA nanocomposites with different HSNs content were attained.

2.4 Characterization

A JEOL JEM-F200 Transmission Electron Microscope (TEM) was used to observe the micrographs and dispersion of nanoparticles in solvent and organic matrix, also observing the lattice of ZnO nanoparticles. The particle size distribution and surface potential of nanoparticles were investigated by a

MALVERN Zetasizer Nano ZS90 laser particle size analyzer. The particle size of HSNs was estimated by measuring the sizes of at least 300 particles in the TEM images by image analysis and processing software (Image-Pro Plus 6.5, Media Cybernetics Inc., USA). X-ray diffraction (XRD) patterns and FTIR spectra of the nanoparticles were examined on a SHIMADZU 6000 X-ray diffractometer in the scanning range from 10° to 80° and Vector 70 FTIR Spectrometer in the wavelength range of 4000~400 cm^{-1} respectively. Transmittance of composite materials was measured by UV-visible spectrophotometer in the wavelength of 300~800 nm. Thermogravimetric analysis (TGA) was examined on a TGA2-SF Thermo- gravimetric Analyzer at a heating rate of 10°C/min in N_2. The refractive index of HSNs dispersion was measured by Abbe refractometer (Abbemat 300/500). The haze and refractive index of HSNs/PVA nanocomposites were tested by Transmittance/Haze tester (WGT-S) and ellipsometer (UVSEL, HORIBA, France) respectively.

3. Results and discussion

3.1 Reaction mechanism

HSNs are prepared by hard template method in reverse microemulsion. In a typical process, as shown in Fig. 1a, ZnO nanoparticles mentioned above as the hard templates are prepared firstly. In order to form a SiO_2 layer on the surface of ZnO nanoparticles, a surface modification step for ZnO nanoparticles is applied, which can change the surface functionality such as surface charge and polarity. SiO_2 with the negative charges are gradually deposited on the surface of ZnO nanoparticles with the positive charges by electrostatic attraction, and then the ZnO@SiO_2 nanoparticles with a core-shell structure are formed. Next, ZnO nanoparticles are corroded gradually by $NH_3 \cdot H_2O$ diffusing to the ZnO surface through the SiO_2 shell. Eventually HSNs are attained and can be monodispersed in water or organic solvents by the subsequent surface modification process. In the formation of ZnO@SiO_2 nanoparticles, the friendly compatibility between the template surface and the shell material allows for a quick and efficient capture of shell material molecules by template, and reliable deposition on this heterogeneous surface is a necessary guarantee for the formation of the core-shell structure.[12,18] During the next stage of template removal, SiO_2 molecules form a stably physical shell structure. $NH_3 \cdot H_2O$ diffuses to the surface of ZnO template through the SiO2 shell to corrode template gradually and finally it is completely removed without any effect on the shell microstructure of the final product.[12,19]

The inverse microemulsion is composed of water as the disperse phase and cyclohexane as the continuous oil phase. The emulsifier is Igepal CO-630, contributing to the formation of a stable water-in-oil emulsion, as shown in Fig. 1b. Under the high gravity circumstance in RPB, water is broken into nanoscale droplet phases used as nanoreactors by the great shearing forces, therefore reversed-phase microemulsion is transparent and has obvious advantages in the synthesis of high-quality hollow nanoparticles.[19] ZnO nanoparticles are monodispersed in water nuclear and TMOS precursor is dissolved in cyclohexane. Moreover, $NH_3 \cdot H_2O$ is selected as hydrolysis catalyst, and meanwhile as the etchant for template agent. TMOS in oil phase hydrolyzes at the oil-water interface under the catalytic effect of $NH_3 \cdot H_2O$ in water and the hydrolysis products enter into water nuclear for heterogeneous nucleation on the surface of ZnO nanoparticles.[20,21] When TMOS dispersed in the oil phase tends to enter the water phase, it must overcome the interfacial resistance through the oil-water interface, which greatly limits the diffusion rate of TMOS and effectively controls the concentration of hydrolysis products in the water core.[22] In this way, the occurrence of homogeneous nucleation is avoided, and the heterogeneous nucleation process can occur in an orderly way.[21] The amount of water in microemulsion is small, so the number of ZnO nanoparticles is strictly limited by the restricted volume of the aqueous phase nanoreactor. The hydrolysis reaction rate of TMOS can be controlled to achieve the uniform coating of SiO_2 on ZnO. At the same time, ZnO nanoparticles are corroded slowly and gradually by $NH_3 \cdot H_2O$ in water. After 2 h reaction, modifier such as PVP dissolved in water is dropwise added and coated on the surface of SiO_2 by *in-situ* modification method. After forming a dense SiO_2 layer, the ZnO template disappears and a hollow structure is formed. And thus, the modified HSNs are finally obtained. The whole preparation process is performed in RPB, which can produce high gravity environment (tens to hundreds of g) by centrifugal force. The process in the RPB reactor is significantly intensified, and it is helpful for providing a more even emulsion system and reaction surrounding, which is suitable for the preparation of uniform nanoparticles at a large-scale.[23,24]

3.2 Characterization of ZnO for template agent

As a template, the prepared ZnO nanoparticles have a spheroid morphology (Fig. 2a), which can be monodispersed in water to form a transparent nanodispersion. Clear and continuous lattice fringes of ZnO nanoparticles with 0.28 nm lattice spacing in the high resolution transmission electron microscopy image (inset 2 of Fig. 2a) correspond to the (100) crystal plane of ZnO, which indicates the ZnO nanocrystals are well crystallized.[25] The average diameter of nanoparticles

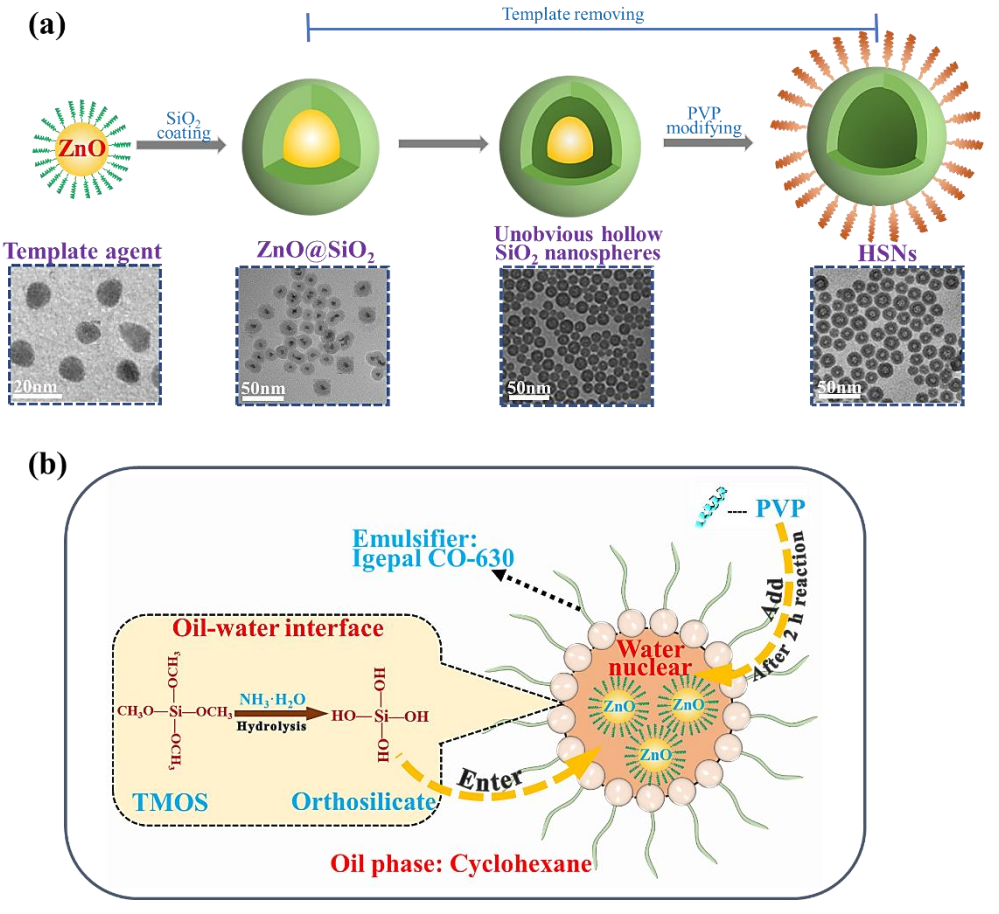

Fig. 1 Diagram of formation process of HSNs by hard template method (a) and reaction mechanism diagram for TMOS in reverse microemulsion (b).

is about 9 nm and the size distribution is very narrow (Fig. 2b). The visual photo of 10 wt% ZnO nanodispersion (inset of Fig. 2b) shows that it after the storage of 2 months, which indicates that the prepared ZnO nanoparticles have excellent dispersion stability in water. XRD patterns of ZnO nanoparticles (Fig. 2c) present all the peaks of unmodified and modified samples expectedly corresponding to hexagonal wurtzite crystal form (JCPDS No.361451).[25,26] All peaks of the modified sample are slightly broadened and weakened than unmodified one, because organic modifier molecules coated on the nanoparticles surface weaken the detection of ZnO crystal components.[25]

The FTIR spectrum of ZnO nanoparticles (Fig. 2d) shows that KH550 has been successfully grafted onto the surface of nanoparticles because its characteristic absorption peaks appear in the curve of modified ZnO such as -CH- (~2947 cm^{-1}), $-CH_2$ (~1220 cm^{-1}) and $-NH_2$ (~1587 cm^{-1}).[27] The absorption peak at ~3428 cm^{-1} corresponds to the characteristic peaks of -OH stretching vibration. TGA results (Fig. 2e) further confirm that ZnO nanoparticles are wrapped by the modifier. The total weight loss rate of unmodified and modified ZnO is 6.5 wt% and 25.1 wt%, respectively. Combined with the results of FT-IR (Fig. 2d), the weight loss of unmodified and modified ZnO nanoparticles in the TGA curves are respectively ascribed to the elimination of -OH bonds and decomposition of KH550 on the surface of nanoparticles.[25,26] Therefore, the total loading of modifier is 18.6%. Moreover, it is noted that surface amination treatment makes ZnO nanoparticles positively charged up to 34.2 mV, which facilitates coating process of SiO_2 with negative charge.[28]

3.3 Influencing factors of preparing HSNs

The effects of different preparation conditions on the morphology and dispersibility of HSNs were investigated and the results show that molar ratio of $NH_3 \cdot H_2O$ to ZnO is the most critical factor to form an obvious hollow structure in the preparation process. TEM images of SiO2 nanoparticles prepared in RPB at different molar ratio of $NH_3 \cdot H_2O$ to ZnO (Figs. 3a-d) have presented that SiO2 nanoparticles undergo a transition from a solid structure to an inconspicuous hollow structure, then to an obvious hollow structure and final to a core-shell structure with the value decreasing from 7.7 to 3.7. More $NH_3 \cdot H_2O$ will corrode ZnO rapidly and SiO_2 nucleates

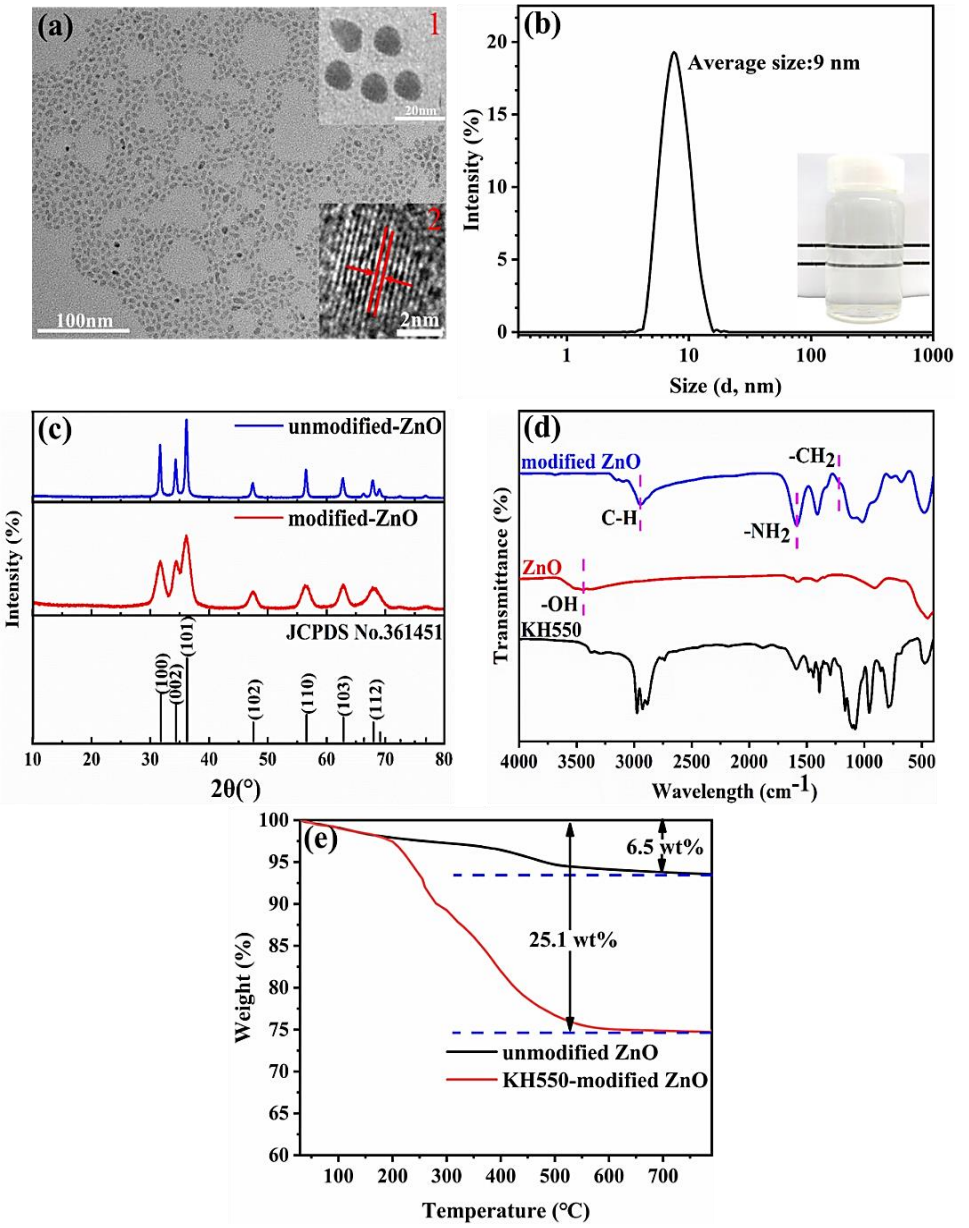

Fig. 2 TEM image (a) of ZnO nanoparticles. Insets include local enlarged view of TEM image and HRTEM image. Particle size distribution (b) of ZnO nanoparticles. Inset includes visual photograph of ZnO nanodispersion. XRD patterns (c) of ZnO nanoparticles. FTIR spectra (d) of ZnO nanoparticles and KH550. TGA curves (e) of ZnO nanoparticles.

independently. Less $NH_3 \cdot H_2O$ cannot corrode ZnO effectively, leading to formation ZnO@SiO_2 nanoparticles with a core-shell structure instead. Under the optimum ratio of 6.1, the deposition rate matches the corrosion rate of template, and the product can be prepared with high uniformity and well-controlled hollow morphology.

In addition, the reaction time has also an important influence on the morphology of nanoparticles. TEM images of nanoparticles prepared in RPB at different reaction times (Figs. 4a-d) present the transition from a core-shell structure to a hollow structure. Since the coated silica shell will slow down the diffusion rate of $NH_3 \cdot H_2O$ to the surface of ZnO nanoparticles, the reaction time of 1 h is not sufficient to corrode ZnO templates to form a core-shell structure nanospheres (Fig. 4a). When the reaction time is extended to 2 h, ZnO nanoparticles are corroded slightly and an unobvious hollow structure can be seen (Fig. 4b). The nanospheres with an obvious hollow structure are obtained when the reaction time is over 3 h (Figs. 4c and 4d).

The effect of rotating speed of RPB on the morphology of SiO_2 were investigated, and the results are presented in Fig. 5. With the increase in rotating speed, the morphology of SiO_2 is from solid to hollow. Mass transfer and mixing efficiency is not enough high at low rotating speeds, resulting in that the formation rate of SiO_2 is slower than the corrosion rate of template, so SiO_2 nanoparticles is mainly solid (Fig. 5a). With

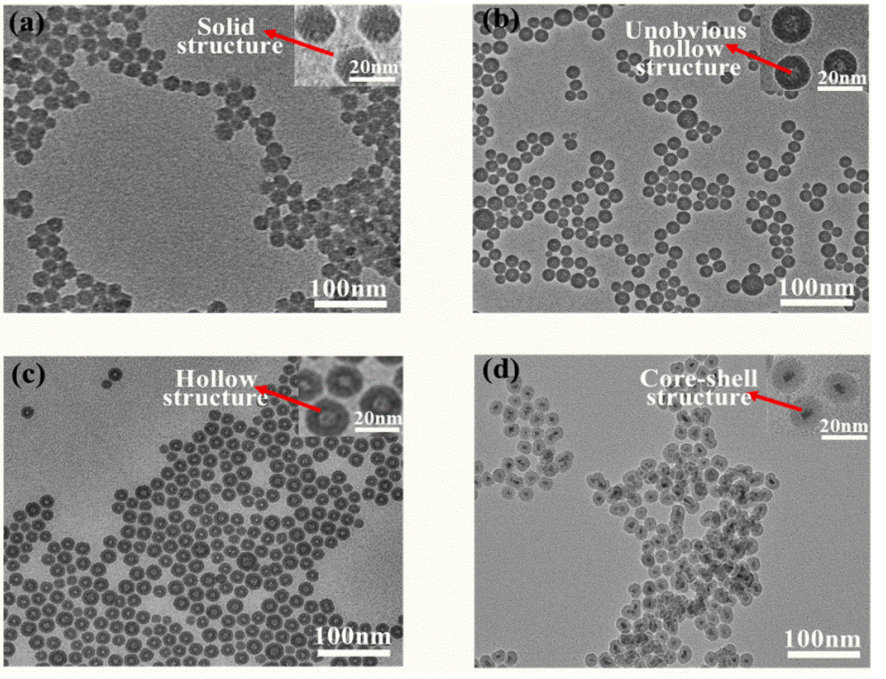

Fig. 3 TEM images of SiO_2 nanoparticles prepared in RPB at molar ratio of 7.7 (a), 6.9 (b), 6.1 (c) and 3.7 (d) for $NH_3 \cdot H_2O$ and ZnO. Inset includes local enlarged views of TEM images.

the increase in the rotating speeds, the apparent reaction rate of SiO_2 is raised. When the rotating speed is higher than 1500 rpm, the prepared SiO_2 nanospheres have an obvious hollow structure (Figs. 5b and c).

The temperature during the whole process including synthesis and modification is constant and has a great effect on the dispersion state of HSNs in water. TEM images of HSNs prepared in RPB at the temperature of 5 °C (Fig. 6a) shows the products fail to exhibit well-dispersed state. It is well known that the viscosity of PVP aqueous solution is in negatively correlated with temperature.[29] At a low temperature of 5°C, PVP coated on the surface of HSNs tends to stick together with gelation. Therefore the final product is troubled by the secondary agglomeration,[30] resulting in the HSNs dispersion becoming opaque (inset of Fig. 6a). TEM images of HSNs prepared at the temperature of 20 °C, 35 °C and 50 °C (Figs. 6b-d) show that the agglomeration of HSNs intensifies with the increase in temperature. When the

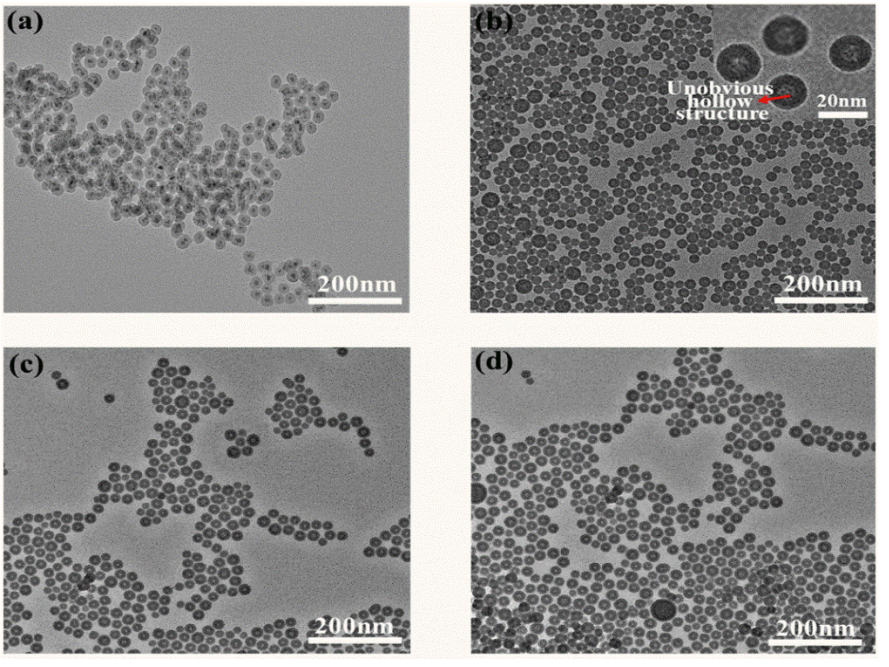

Fig. 4 TEM images of SiO_2 nanoparticles prepared in RPB at reaction time of 1h (a), 2h (b), 3h (b) and 4h (b). Inset in Fig. 4b includes local enlarged view of TEM image.

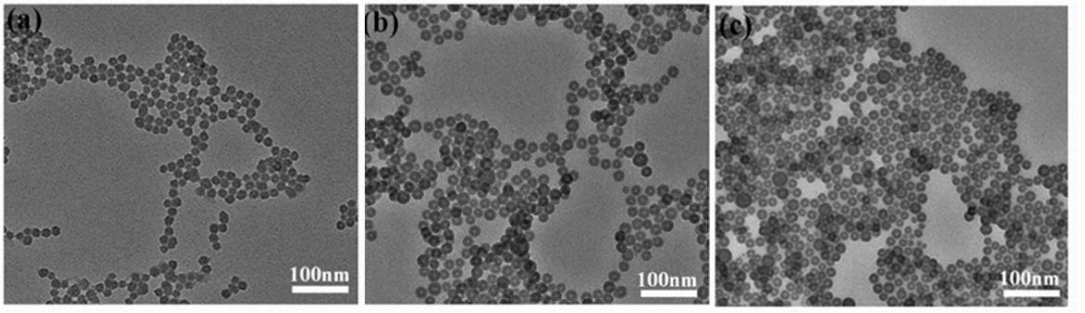

Fig. 5 TEM images of HSNs prepared in RPB at rotational speeds of 500 rpm (a), 1500 rpm (b), 2500 rpm (c).

temperature is 20 °C, the surface of HSNs can be effectively coated by modifier PVP to form a dense capped layer, causing a good dispersion of HSNs in water to form a high transparent dispersion (inset of Fig. 6b). However, the dispersibility of HSNs becomes worse with rising temperatures and the nanodispersions gradually appear opaque and whitish (insets of Figs. 6c and 6d). The particle size distributions are also tested by a laser particle analysis, and the results are shown in Fig. 6e. The HSNs prepared at 20 °C have a minimum average particle size with an extremely narrow size distribution, indicating that they have the best state of dispersion in water. Moreover, the dispersions of HSNs in different organic solvents were also synthesized successfully and used to fabricate the highly transparent nanocomposites by the solution blending method, which can further expand the application fields of HSNs. Herein, HSNs modified by

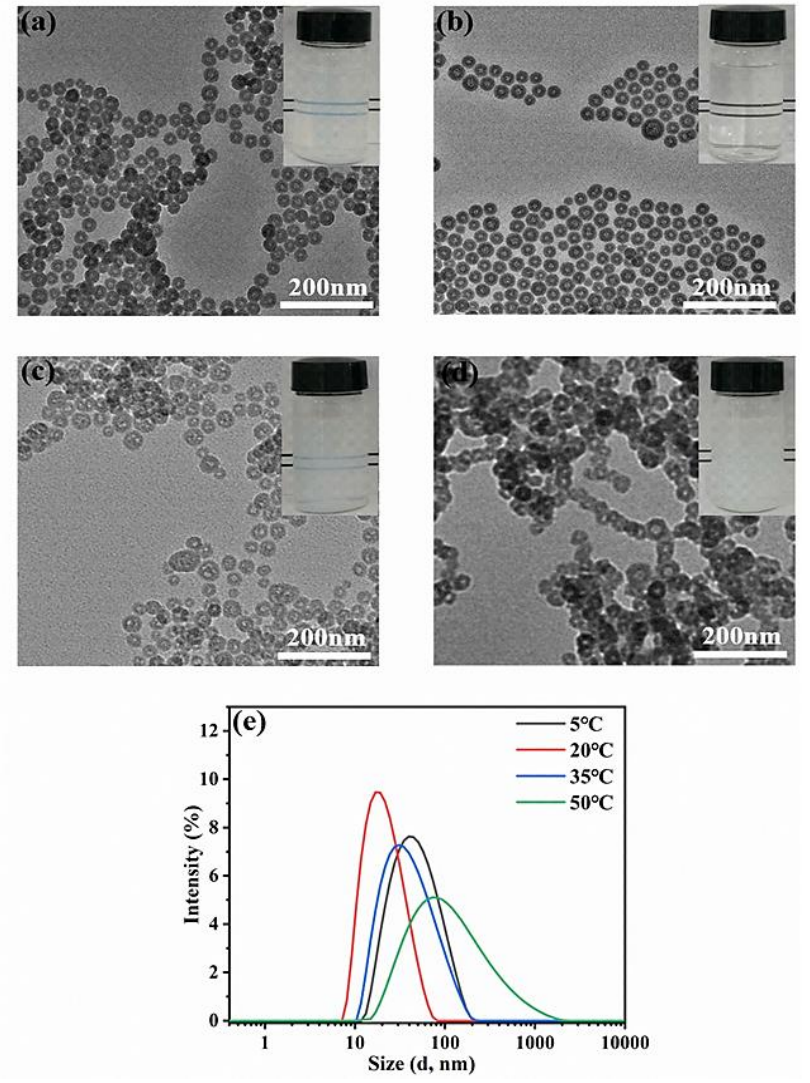

Fig. 6 TEM images of HSNs prepared in RPB at temperatures of 5 °C (a), 20 °C (b), 35 °C (c), 50 °C (d). Inset includes visual photographs of HSNs dispersions. Particle size distribution (e) of HSNs prepared at different temperatures.

different types of modifiers such as PVP, KH570, and KH590 can be stably well-dispersed in corresponding solvents (water, MIBK and MeOH) to form the transparent dispersions, respectively.

Processing capacity of RPB reactor for synthesis of such HSNs mentioned above is from ten to hundreds of grams per batch in the laboratory. In this study, the gram-level preparation of HSNs in STR and RPB was investigated for comparison. The nanoparticles synthesized in RPB are uniform hollow structure with regular morphology (Fig. 7a). After modified by PVP, they can be well-dispersed in water to attain highly transparent nanodispersion (inset of Fig. 7a). Unfortunately, the products prepared in STR are solid and hollow mixtures (Fig. 7b), and further prolongation of reaction time has no improvement in the uniformity of structure. The particle size distribution of SiO2 nanoparticles and their cavity size synthesized in RPB or STR have been analyzed (Figs. 7c-d). SiO_2 nanoparticles prepared in RPB have an average diameter of about 20 nm and a narrow size distribution from 10 to 30 nm, which are obviously smaller and more uniform than those prepared in STR. Furthermore, the inner cavity of SiO_2 is even and the size is about 8 nm, but most nanoparticles prepare in STR are solid. More importantly, the reaction time in RPB is 3 h as half as that in STR, resulting from the formation of uniform water-in-oil emulsions with smaller size of water phase and faster mass transfer at oil-water interface in RPB.[24] Moreover, the yields (mass percentage of the well-dispersed nanoparticles in the total output) of HSNs in RPB and STR with the morphology as shown in Figs. 6a and 6b have a huge difference. The yield in RPB is beyond 75%, which is twice as much as that in STR. All in all, the high gravity technology provides the possibility for the large scale-up preparation of ultrafine HSNs, which is important for the industrial application of HSNs as antireflection functional additive in optical polymer matrices.

3.4 Analysis of characterization results about HSNs

From the FT-IR spectra of HSNs (Fig. 8a), it can be seen that unmodified HSNs has no C-H (～2969 cm^{-1}), C=O (～1644 cm^{-1}) and C-N (～1398 cm^{-1}) peaks, which are the characteristic absorption peaks of PVP. These peaks appear in the modified ones, indicating that PVP are successfully wrapped on HSNs. However, there is no new characteristic absorption peak, illustrating only existence of physical interaction between PVP and HSNs. Moreover, there are a large number of OH groups on the surface of HSNs and the stretching vibration peak appears at ～3384 cm^{-1}. XRD pattern of HSNs (Fig. 8b) exhibits only one wide diffraction peak at about 25°, indicating that the HSNs present an amorphous state. In the TGA curves (Fig. 8c), the total weight loss of unmodified and modified HSNs are 5.9 wt% and 21.8 wt % respectively. Combined with the results of FT-IR, they

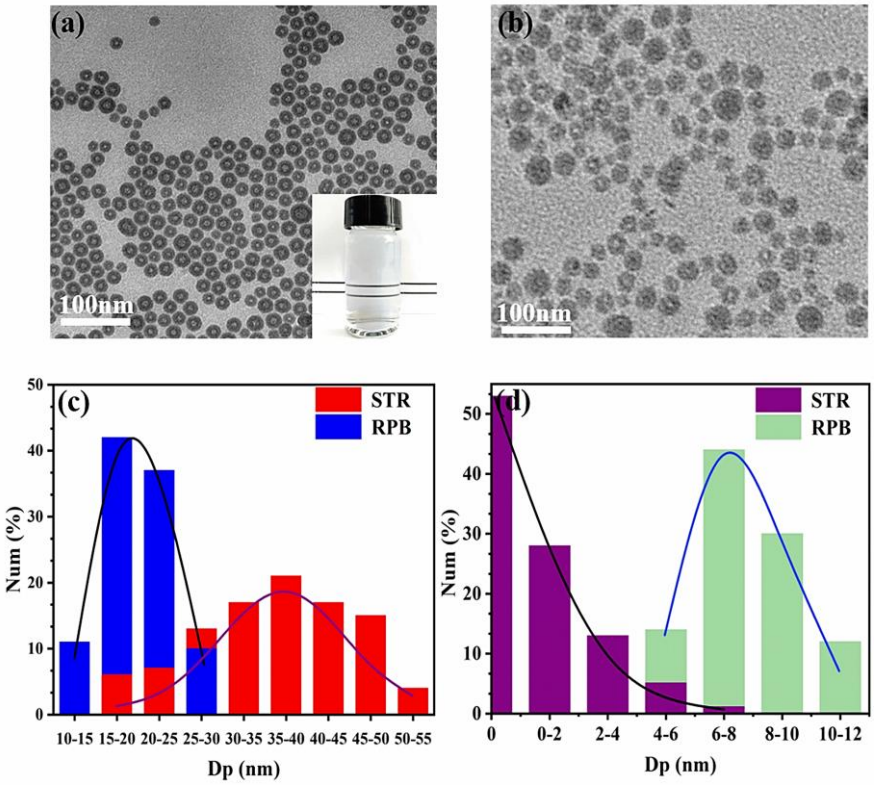

Fig. 7 TEM images of HSNs prepared in RPB (a) and STR (b). Inset in Fig. 6a includes visual photograph of HSNs nanodispersion. Histogram of particle size distribution (c) and inner cavity size (d) of HSNs prepared in RPB and STR respectively.

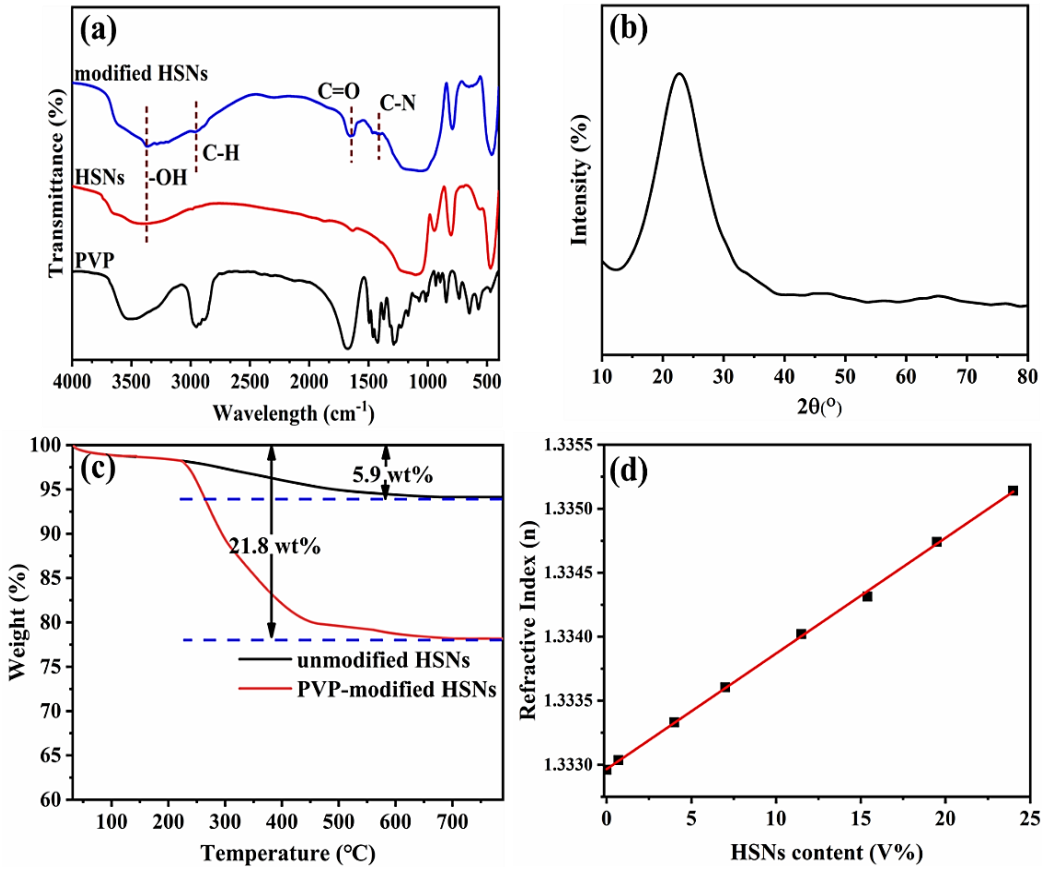

Fig. 8 FT-IR spectra (a) of HSNs and PVP. XRD pattern (b) and TGA curves (c) of HSNs. Refractive index (d) of aqueous HSNs dispersions with different contents of HSNs.

are mainly due to elimination of OH bonds and decomposition of PVP on the surface of HSNs. The coating amount of PVP is about 15.9 wt%.

The influence of HSNs volume fraction in water on the refractive index of HSNs dispersions was investigated. The relationship of them can be calculated using the Equation 1.[16,31]

$$n_t = n_1 V\% + n_2(1 - V\%) = (n_1 - n_2)V\% + n_2 \quad (1)$$

where n_t, n_1 and n_2 are refractive index of HSNs aqueous dispersion, HSNs and H_2O respectively. V% is volume fraction of HSNs in water. The value of n_t can be measured using a refractometer and the results are presented in Fig. 8d. It has a linear relationship with the content of HSNs in water. n_2 is about 1.333 and the slope of the line is 0.009. The function of n_t and V% is fitted linearly (R^2=0.999), namely n_t=0.009V%+1.333. So, the refractive index of HSNs (n_1) is 1.342, which is much lower than that of most polymers. Moreover, the refractive index of HSNs also can be calculated from their size. According to Equation 1, n_t, n_1 and n_2 are refractive index of HSNs, solid SiO_2 and air. As we know n_1 and n_2 are about 1.46 and 1 respectively. The shell of HSNs has high porosity. According to the literatures,[32,33] pore volume of the amorphous SiO_2 is generally about 0.12 cm^3/g. And the ratio of pore volume of the HSNs shell to the whole volume of HSNs can be calculated at 17%, based on the specific volume of 0.73 cm^3/g (density of 1.37 g/cm^3) for HSNs. Considering inner cavity volume fraction of 7%, the total porosity of HSNs is about 24% and theoretical refractive index is 1.35, which shows the theoretical calculation result is in good agreement with experimental one. This also indicates that cavity of HSNs is fully filled with air instead of water. Otherwise, the calculated and measured value of refractive index for HSNs should be 1.430. In addition, it is satisfactory that the modified HSNs in water are endowed with excellent dispersion stability. The nanodispersions have maintained good transparency without sediments after placed several months, due to strong charge repulsion effect among HSNs (-19.2 mV).

3.5 Optical performance of HSNs/PVA nanocomposites

HSNs/PVA nanocomposite films with the thickness of 100 μm have been fabricated by the solution blending method. From the UV-vis transmittance spectra of neat PVA and HSNs/PVA nanocomposites (Fig. 8a), it is can be seen that the transmittance of visible light is enhanced remarkably with the rise in HSNs content, illustrating that HSNs indeed are well-

dispersed in PVA matrix. Therefore, the nanocomposites have an excellent antireflection effect. In addition, HSNs/PVA nanocomposite remains high transparency without a whitish or opaque appearance (inset of Fig. 9a). The visible transmittance and haze at 580 nm of the films are clearly depicted in Fig. 9b. When HSNs content increases from 0 to 33 wt%, the transmittance increases from 91.5% to 98%, because the well-dispersed HSNs can decrease surface reflectivity and boost total luminous flux of nanocomposites due to their low refractive index. However, as we know, due to the existence of difference in refractive index between nanoparticles and polymer, if the nanoparticles aggregate or have larger size in polymer matrix, they can change the optical path more or less and cause the light diffuse scattering (Rayleigh scattering). Although the surface reflection ratio declines because of the deduction in refractive index of nanocomposites, the total reflectivity may be enhanced, and the haze of nanocomposite must be increased, which is a huge obstacle for the application of antireflection transparent composite films.[9,16] When the particles size is bigger and particles aggregation is more, the haze of composites is raised more obviously. To our surprise, the haze of prepared HSNs/PVA nanocomposite is increased slightly with the addition of HSNs, indicating the excellent dispersion state of HSNs in PVA matrix. TEM image of nanocomposite (Fig. 9c) indeed confirms that HSNs with 22 wt% content have a homogeneous dispersion in PVA matrix without any aggregations. Light diffuse scattering does not happen because the nanoparticles have the size of much less than 40 nm and are well-dispersed in optical polymer matrix basically.[16] In this way, it gives full play to the function of anti-reflection and remarkably improves optical performance of nanocomposites without diffuse reflection.

The influences of HSNs volume fraction on the refractive index of HSNs/PVA nanocomposites are investigated through theoretical calculation and experimental test respectively, as shown in Fig. 9d. The theoretical values were also calculated according to Equation 1. n_t, n_1 and n_2 are refractive index of HSNs/PVA, HSNs and PVA respectively. n_1 is 1.342 as mentioned above and n_2 equals to 1.53, which is the theoretical value of pure PVA. Therefore, when the volume fraction of HSNs reaches 21%, n_t can enhance linearly to 1.49. However, with the same content of HSNs, the refractive index of HSNs/PVA nanocomposites tested in the experiment is lower than that by calculation. It is decreased nonlinearly from 1.535 to 1.458 with increased HSNs content from 0 to 21 vol%,

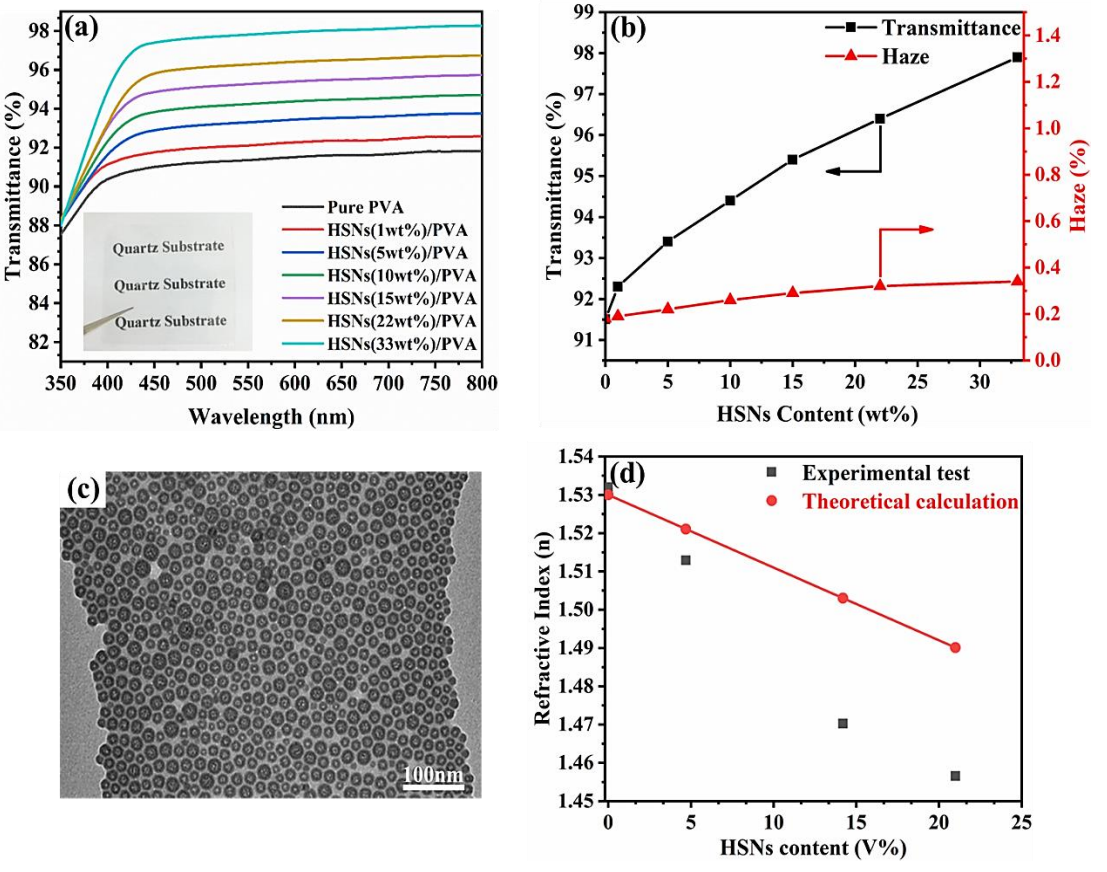

Fig. 9 UV-visible transmittance spectra (a) of films with different HSNs contents. Inset includes visual photograph of HSNs/PVA film. Transmittance and haze at 580 nm (b) of HSNs/PVA nanocomposites with different HSNs contents. TEM image (c) of HSNs/PVA nanocomposites with 22 wt% HSNs. Refractive index (d) of HSNs/PVA nanocomposites with different HSNs contents.

which is not consistent with the theoretical calculation results,[31] because the addition of inorganic nanoparticles would reduce the crystallinity of the organic substrate.[34]

All these indicate that the HSNs/PVA composite materials have outstanding optical performance with considerable application prospect. Of course, by changing the types of modifiers, the HSNs can be incorporated into the different organic substrates by the simple blending method to form nanocomposites with excellent optical properties.

4. Conclusion

In summary, the synthesis of 20 nm HSNs with the inner cavity diameter of 8 nm has been scaled up successfully in RPB. These nanoparticles show a very uniform particle size and an excellent dispersity. As the anti-reflection additive agent, they have been introduced into the optical PVA matrix by a simple solution blending method. HSNs can reduce the refractive index and improve the visible transmittance of PVA effectively. Most importantly, the haze of PVA is unchanged basically by adding HSNs, indicating that HSNs are well-dispersed in polymer matrix. This work provides a simple and effective method to stably synthesize the ultrafine HSNs and super transparent inorganic/organic nanocomposites, which can promote the development of the technology for the large-scale preparation and industrial application of anti-reflection materials.

Acknowledgement

This work was financially supported by National Natural Science Foundation of China 21776016.

Conflict of Interest

There is no conflict of interest.

Supporting Information

Not applicable.

References

[1] T. Ma, X. Yu, H. Li, W. Zhang, X. Cheng, W. Zhu, X. Qiu, High volumetric capacity of hollow structured SnO_2@Si nanospheres for lithium-ion batteries, *Nano Letters*, 2017, **17**, 3959-3964, doi: 10.1021/acs.nanolett.7b01674.

[2] X. W. David Lou, L. A. Archer, Z. Yang, Hollow micro-/nanostructures: synthesis and applications, *Advanced Materials*, 2008, **20**, 3987-4019, doi: 10.1002/adma.200800854.

[3] B. Li, H. C. Zeng, Architecture and preparation of hollow catalytic devices, *Advanced Materials*, 2019, **31**, 1801104, doi: 10.1002/adma.201801104.

[4] X. Wang, J. Feng, Y. Bai, Q. Zhang, Y. Yin, Synthesis, properties, and applications of hollow micro-/ nanostructures, *Chemical Reviews*, 2016, **116**, 10983-11060, doi: 10.1021/acs.chemrev.5b00731.

[5] L. Yu, X. Y. Yu, X. W. David Lou, The design and synthesis of hollow micro-/ nanostructures: present and future trends, *Advanced Materials*, 2018, **30**, 1800939, doi: 10.1002/adma.201800939.

[6] J. Dai, H. Zou, Z. Shi, H. Yang, R. Wang, Z. Zhang, S. Qiu, Janus N-doped Carbon@Silica hollow spheres as multifunctional amphiphilic nanoreactors for base-free aerobic oxidation of alcohols in water, *ACS Applied Materials & Interfaces*, 2018, **10**, 33474-33483, doi: 10.1021/acsami.8b11888.

[7] F.-P. Chang, Y. Hung, J.-H. Chang, C.-H. Lin, C.-Y. Mou, Enzyme encapsulated hollow silica nanospheres for intracellular biocatalysis, *ACS Applied Materials & Interfaces*, 2014, **6**, 6883-6890, doi: 10.1021/am500701c.

[8] J. Zhang, L. Ai, S. Lin, P. Lan, Y. Lu, N. Dai, R. Tan, B. Fan, W. Song, Preparation of humidity, abrasion, and dust resistant antireflection coatings for photovoltaic modules via dual precursor modification and hybridization of hollow silica nanospheres, *Solar Energy Materials and Solar Cells*, 2019, **192**, 188-196, doi: 10.1016/j.solmat.2018.12.032.

[9] J. Loste, J.-M. Lopez-Cuesta, L. Billon, H. Garay, M. Save, Transparent polymer nanocomposites: an overview on their synthesis and advanced properties, *Progress in Polymer Science*, 2019, **89**, 133-158, doi: 10.1016/j.progpolymsci.2018.10.003.

[10] W. Suthabanditpong, C. Takai, M. Fuji, R. Buntem, T. Shirai, Improved optical properties of silica/UV-cured polymer composite films made of hollow silica nanoparticles with a hierarchical structure for light diffuser film applications, *Physical Chemistry Chemical Physics*, 2016, **18**, 16293-16301, doi: 10.1039/c6cp01005a.

[11] L. Ernawati, T. Ogi, R. Balgis, K. Okuyama, M. Stucki, S. C. Hess, W. J. Stark, Hollow silica as an optically transparent and thermally insulating polymer additive, *Langmuir*, 2016, **32**, 338-345, doi: 10.1021/acs.langmuir.5b04063.

[12] J. Hu, M. Chen, X. Fang, L. Wu, Fabrication and application of inorganic hollow spheres, *Chemical Society Reviews*, 2011, **40**, 5472, doi: 10.1039/c1cs15103g.

[13] J. Wang, Y. Cui, D. Wang, Design of hollow nanostructures for energy storage, conversion and production, *Advanced Materials*, 2019, **31**, 1801993, doi: 10.1002/adma.201801993.

[14] G. Prieto, H. Tüysüz, N. Duyckaerts, J. Knossalla, G.-H. Wang, F. Schüth, Hollow nano- and microstructures as catalysts, *Chemical Reviews*, 2016, **116**, 14056-14119, doi: 10.1021/acs.chemrev.6b00374.

[15] G. Y. Jia, Z. H. Ji, H. N. Wang, R. Y. Chen, Preparation and properties of five-layer graded-refractive-index antireflection coating nanostructured by solid and hollow silica particles, *Thin*

Solid Films, 2017, **642**, 174-181, doi: 10.1016/j.tsf.2017.09.038.
[16] H. Althues, J. Henle, S. Kaskel, Functional inorganic nanofillers for transparent polymers, *Chemical Society Reviews*, 2007, **36**, 1454-1465, doi: 10.1039/b608177k.
[17] J. F. Chen, J. Y. Zhang, Z. G. Shen, J. Zhong, J. Yun, Preparation and characterization of amorphous cefuroxime axetil drug nanoparticles with novel technology: high-gravity antisolvent precipitation, *Industrial & Engineering Chemistry Research*, 2006, **45**, 8723-8727, doi: 10.1021/ie060445h.
[18] Q.-Q. Jin, C.-Y. Zhang, W.-N. Wang, B.-J. Chen, J. Ruan, H.-S. Qian, Recent development on controlled synthesis of metal sulfides hollow nanostructures *via* hard template engaged strategy: a mini-review, *The Chemical Record*, 2020, **20**, 882-892, doi: 10.1002/tcr.202000033.
[19] S. Wolf, C. Feldmann, Microemulsions: options to expand the synthesis of inorganic nanoparticles, *Angewandte Chemie International Edition*, 2016, **55**, 15728-15752, doi: 10.1002/anie.201604263.
[20] H. Kang, D. J. Long, C. L. Haynes, Preparation of colloidally stable positively charged hollow silica nanoparticles: effect of minimizing hydrolysis on ζ potentials, *Langmuir*, 2019, **35**, 7985-7994, doi: 10.1021/acs.langmuir.9b01042.
[21] G. C. Sosso, J. Chen, S. J. Cox, M. Fitzner, P. Pedevilla, A. Zen, A. Michaelides, Crystal nucleation in liquids: open questions and future challenges in molecular dynamics simulations, *Chemical Reviews*, 2016, **116**, 7078-7116, doi: 10.1021/acs.chemrev.5b00744.
[22] B. Richard, J.-L. Lemyre, A. M. Ritcey, Nanoparticle size control in microemulsion synthesis, *Langmuir*, 2017, **33**, 4748-4757, doi: 10.1021/acs.langmuir.7b00773.
[23] D. Wenzel, A. Gorak, Review and analysis of micromixing in rotating packed beds, *Chemical Engineering Journal*, 2018, **345**, 492-506, doi: 10.1016/j.cej.2018.03.109.
[24] H. Liu, T. Hu, D. Wang, J. Shi, J. Zhang, J.-X. Wang, Y. Pu, J.-F. Chen, Preparation of fluorescent waterborne polyurethane nanodispersion by high-gravity miniemulsion polymerization for multifunctional applications, *Chemical Engineering and Processing - Process Intensification*, 2019, **136**, 36-43, doi: 10.1016/j.cep.2018.12.012.
[25] C.-W. Cui, C. Yang, J. Bao, X.-J. Huang, X.-F. Zeng, J.-F. Chen, Monodispersed ZnO nanoparticle-poly(methyl methacrylate) composites with visible transparency for ultraviolet shielding applications, *ACS Applied Nano Materials*, 2020, **3**, 9026-9034, doi: 10.1021/acsanm.0c01723.
[26] X.-J. Huang, X.-F. Zeng, J.-X. Wang, L.-L. Zhang, J.-F. Chen, Synthesis of monodispersed ZnO@SiO_2 nanoparticles for anti-UV aging application in highly transparent polymer-based nanocomposites, *Journal of Materials Science*, 2019, **54**, 8581-8590, doi: 10.1007/s10853-019-03393-z.
[27] H. Shi, Y. He, Y. Pan, H. Di, G. Zeng, L. Zhang, C. Zhang, A modified mussel-inspired method to fabricate TiO_2 decorated superhydrophilic PVDF membrane for oil/water separation, *Journal of Membrane Science*, 2016, **506**, 60-70, doi: 10.1016/j.memsci.2016.01.053.
[28] T. Gao, B. P. Jelle, L. I. C. Sandberg, A. Gustavsen, Monodisperse hollow silica nanospheres for nano insulation materials: synthesis, characterization, and life cycle assessment, *ACS Applied Materials & Interfaces*, 2013, **5**, 761-767, doi: 10.1021/am302303b.
[29] R. Sadeghi, M. Taghi Zafarani-Moattar, Thermodynamics of aqueous solutions of polyvinylpyrrolidone, *The Journal of Chemical Thermodynamics*, 2004, **36**, 665-670, doi: 10.1016/j.jct.2004.04.008.
[30] J. Li, K. Inukai, Y. Takahashi, W. Shin, Synthesis and size control of monodispersed $BaTiO_3$-PVP nanoparticles, *Journal of Asian Ceramic Societies*, 2016, **4**, 394-402, doi: 10.1016/j.jascer.2016.09.001.
[31] Y. Xia, C. Zhang, J.-X. Wang, D. Wang, X.-F. Zeng, J.-F. Chen, Synthesis of transparent aqueous ZrO_2 nanodispersion with a controllable crystalline phase without modification for a high-refractive-index nanocomposite film, *Langmuir*, 2018, **34**, 6806-6813, doi: 10.1021/acs.langmuir.8b00160.
[32] L. Kong, A. Uedono, S. V. Smith, Y. Yamashita, I. Chironi, Synthesis of silica nanoparticles using oil-in-water emulsion and the porosity analysis, *Journal of Sol-Gel Science and Technology*, 2012, **64**, 309-314, doi: 10.1007/s10971-012-2859-7.
[33] C. Raschpichler, C. Goroncy, B. Langer, E. Antonsson, B. Wassermann, C. Graf, P. Klack, T. Lischke, E. Rühl, Surface properties and porosity of silica particles studied by wide-angle soft X-ray scattering, *The Journal of Physical Chemistry C*, 2020, **124**, 16663-16674, doi: 10.1021/acs.jpcc.0c04308.
[34] B. Karthikeyan, S. Hariharan, A. Sasidharan, V. Gayathri, T. Arun, A. Akbari-Fakhrabadi, C. Madhumitha, Optical, vibrational and fluorescence recombination pathway properties of nano SiO_2-PVA composite films, *Optical Materials*, 2019, **90**, 139-144, doi: 10.1016/j.optmat.2019.01.063.

